MATERIALS CHEMISTRY
FRONTIERS

RESEARCH ARTICLE

View Article Online
View Journal | View Issue

Cite this: *Mater. Chem. Front.*, 2017, **1**, 2383

Ground-state conformers enable bright single-fluorophore ratiometric thermometers with positive temperature coefficients†

Weijie Chi,[a] Wenting Yin,[b] Qingkai Qi,[b] Qinglong Qiao,[b] Yuyan Lin,[c] Zhuohui Zhu,[c] Sindhu Vijayan,[a] Michinao Hashimoto,[a] Gayathri Udayakumar,[c] Zhaochao Xu *[b] and Xiaogang Liu *[ac]

Received 31st July 2017,
Accepted 28th August 2017

DOI: 10.1039/c7qm00345e

rsc.li/frontiers-materials

Fluorescence thermometry based on organic dyes affords high spatial and temporal resolution with a simple system design and low cost, for measuring temperatures in microenvironments. Many fluorescent thermometers consist of two types of fluorophores with distinct temperature responses, and the ratios of their fluorescence intensities afford accurate temperature information. Yet, the reliability of these ratiometric thermometers is vulnerable to photobleaching induced system variations. In this paper, we have proposed and demonstrated a new strategy, to achieve ratiometric temperature measurements from 15 °C to 75 °C, based on ground-state conformational isomers of a single type of dye. These ground-state conformers emit bright fluorescence, in contrast to excited-state conformational changes that generally quench emissions. Moreover, thermal equilibrium of these conformers and their distinct spectra lead to ratiometric temperature readings that are not affected by photobleaching. We expect that our design strategy has significant implications for developing fluorescence thermometry with outstanding reliability.

Introduction

Organic dye based fluorescent temperature sensors permit dynamic measurement of temperatures with high spatial and temporal resolution.[1,2] Their outstanding resolution and biocompatibility enable a broad range of applications that are impossible with numerous macroscale thermometers. Such applications span from monitoring the whole field temperature distribution in water[3] to revealing heat exchange in microfluidic channels,[4,5] from temperature control in industrial processing[6,7] to heat regulation in biological cells.[8–11] Nevertheless, the long-term reliability of these temperature sensors remains a critical challenge due to unavoidable photobleaching of organic dyes under repetitive laser irradiation.

To address the reliability issues, two main techniques have been developed.[12] Fluorescence lifetime imaging permits accurate measurements that are independent of dye concentrations and laser excitation power. Yet, expensive time-gated electronics and limited temporal resolution in fluorescence-lifetime imaging microscopy (FLIM) render this technique less accessible than fluorescence intensity based measurements.[1] Similarly, by utilizing two types of fluorophores with distinct temperature responses in a thermometer, the ratios of their emission intensities afford reliable temperature measurements that are comparable to FLIM results in principle.[3,13,14] However, due to different environmental sensitivity, photostability and photobleaching rates between these two types of dyes, their relative concentrations change over time and thus greatly compromise the reliability of dual-fluorophore ratiometric sensors. Besides these two main strategies, smart optical designs have also been developed to enhance the reliability of a thermometer. For example, Peter Löw and co-workers used an automated shutter to reduce exposure time to fluorophores, aiming to minimize the impact of photobleaching.[15] Such measures prolong the lifespan of the system, but do not completely solve the reliability issues.

To solve the reliability problem of dual-fluorophore ratiometric sensors, we propose a new strategy that allows the ratiometric measurement of temperatures based on a single type of fluorophore. Fluorophores in a single-fluorophore ratiometric

---

[a] *Singapore University of Technology and Design, 8 Somapah Road, 487372, Singapore. E-mail: xiaogang_liu@sutd.edu.sg*

[b] *Key Laboratory of Separation Science for Analytical Chemistry, Dalian Institute of Chemical Physics, Chinese Academy of Sciences, 457 Zhongshan Road, Dalian 116023, China. E-mail: zcxu@dicp.ac.cn*

[c] *Singapore-MIT Alliance for Research and Technology (SMART), 1 CREATE Way, 138602, Singapore*

† Electronic supplementary information (ESI) available. CCDC 1564212. For ESI and crystallographic data in CIF or other electronic format see DOI: 10.1039/c7qm00345e

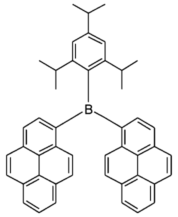

Scheme 1 Molecular structure of dipyren-1-yl(2,4,6-triisopropylphenyl)-borane (**DPTB**).

sensor should possess multiple conformational isomers, which co-exist at the working temperatures of a thermometer and display distinct spectral properties. Consequently, thermal equilibrium between these conformers not only enables ratiometric temperature sensing, but also avoids varied photobleaching rates in dual-fluorophore ratiometric sensors. Moreover, these conformational isomers may collectively endow fluorophores with novel optical properties that are unachievable in many existing organic fluorophores. For example, if increasing temperature raises the population of a more emissive conformer, this fluorophore could display brighter emissions at higher temperatures, or a positive temperature coefficient.[16]

In this paper, we have discussed molecular design considerations to realize single-fluorophore ratiometric imaging. We demonstrate our strategy by employing ground state conformational isomers of **DPTB** to construct a ratiometric fluorescent thermometer (Scheme 1). We show that **DPTB** in combination with a standard digital camera allows reliable determinations of temperatures from 15 °C to 75 °C *via* a simple system design. In addition, we show that multiple conformational isomers of **DPTB** endow it with an unusual positive temperature coefficient in certain solvents [*i.e.*, ethyl acetate (EA) and dimethyl sulfoxide (DMSO)].

Molecular design strategy

Realizing a single-fluorophore ratiometric thermometer requires that a fluorophore possesses multiple emissive conformers. If these emissive conformers demonstrate different fluorescence wavelengths, possess distinct temperature dependence, and are all accessible at the working temperatures of a probe, the ratios of their fluorescence intensities will permit single-fluorophore ratiometric temperature measurements.

Currently, it is well-known that many fluorophores exhibit more than one conformer in the excited state (Fig. 1a). One common phenomenon is the conversion between a local excited (LE) state and a twisted intramolecular charge transfer (TICT) state upon photo-excitation (Fig. 1b).[17] In the LE state, a dye remains nearly flat and highly emissive. In contrast, the TICT state is manifested by a ∼90° twisting between an electron-donating moiety (D) and an electron-accepting moiety (A). The TICT state is typically non-emissive and highly reactive. The other well-known phenomenon is aggregation induced emission (AIE; Fig. 1c).[18,19] AIE molecules are structurally flexible, possessing different conformational isomers *via* intramolecular rotations. Such intramolecular rotations significantly quench the fluorescence of monomer fluorophores, while restricting these rotations in the aggregated state turns on bright fluorescence. In addition to TICT and AIE, several other types of intramolecular rotations/flapping have also been reported.[20,21] However, while intramolecular rotations generate conformational isomers, such rotations also accelerate non-radiative decay, resulting in weak fluorescence signals and sacrificing the feasibility of ratiometric imaging (especially in low-viscosity medium).[19,22] Notably, TICT conformers are also highly reactive, greatly reducing the photostability of fluorophores.[23,24]

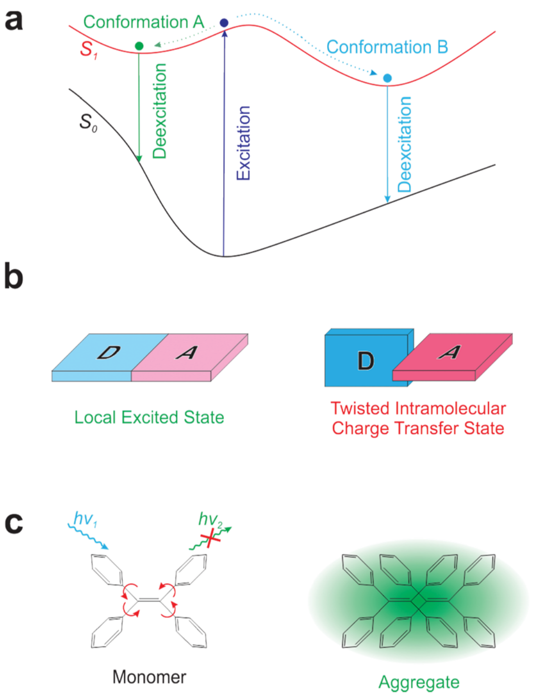

Fig. 1 Schematic illustrations of (a) the potential energy profile, which leads to two states upon photoexcitation of a dye; (b) local excited (LE) and twisted intramolecular charge transfer (TICT) states; and (c) aggregation induced emission.

Given the drawbacks of conformer generation in the excited state, we turn our attention to conformational isomers in the ground state (Fig. 2a). The transition of conformational isomers in the ground state may have a large impact on their electronic structures and optical spectra, but does not directly affect the fluorescence strength of a fluorophore (as fluorescence process starts from the excited state). To this end, numerous conformers of various organic materials and their distinct spectral properties have been reported in the polymer and crystal states.[25–34] A similar phenomenon in the solution phase has also been reported.[35–38] However, these fluorophores in the solution phase have either extremely short wavelengths or poor brightness, limiting their practical applications.

In view of this technical challenge, we examined many fluorophores with the aid of chemical database. Most "classical" fluorophores, such as coumarin, rhodamine, BODIPY, and cyanine dyes, possess a rigid molecular structure and usually exhibit only one electronically equivalent conformer in the ground state.[39]

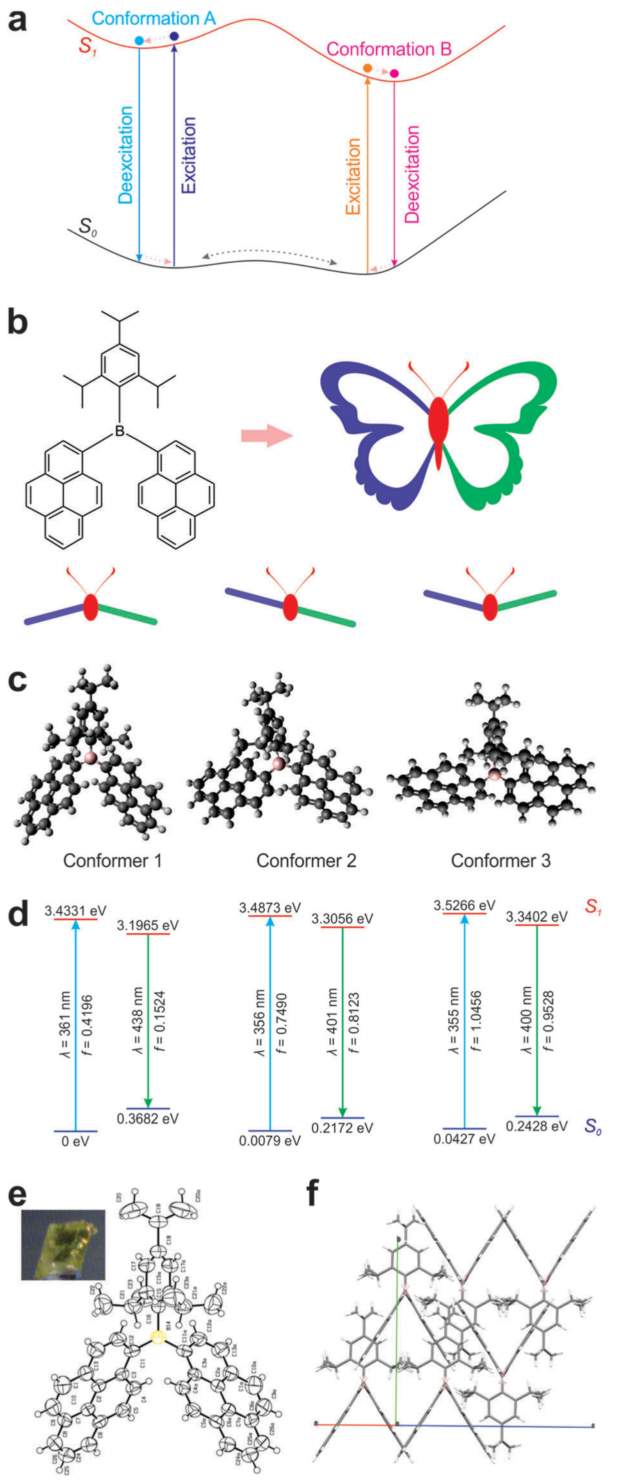

Fig. 2 (a) Schematic illustration of the potential energy profile, which leads to multiple conformational isomers in the ground state; (b) a "butterfly" illustration of the molecular structure and conformational isomers of **DPTB**; (c) optimized molecular structures of three conformational isomers of **DPTB** in the ground state *in vacuo*; (d) relative energy levels of the ground (S_0) and excited (S_1) states for three conformational isomers of **DPTB** during absorption (upward arrows) and emission (downward arrows) processes *in vacuo*; (e) crystallographic asymmetric unit of **DPTB** at room temperature with anisotropic displacement ellipsoids drawn at the 50% probability level; the inset shows a photograph of the single crystal used for the crystallographic experiment; (f) unit cell structure of the **DPTB** crystal.

In contrast, many structurally flexible dyes are non-fluorescent or weakly fluorescent. However, we reason that "pseudo-rigid" fluorophores will lead to multiple conformational isomers in the ground state, while maintaining bright fluorescence. One of such "pseudo-rigid" dyes is **DPTB**, as firstly reported by Yang and co-workers in a seminal work (Scheme 1 and Fig. 2b).[40]

Computational analysis of ground-state conformers

The molecular structure of **DPTB** can be divided into three parts: a 2,4,6-triisopropylphenyl (TIPP) group and two pyrene (Py) units, all connected *via* a boron atom in the center (Fig. 2b). Intuitively, this molecule mimics the structure of a butterfly: the TIPP unit and the boron atom are like the head and body of a butterfly, and the two pyrene units resemble the two wings of a butterfly. By considering the relative positions of "wings" with respect to that of the "head–body", we reason that there are at least three distinct conformations in this **DPTB** "butterfly": down–down, up–down, and up–up conformations.

Indeed, our conformational search using DFT calculations reproduces all three conformers of **DPTB** (Fig. 2c and Fig. S1, S2, ESI†). Our calculations show that Conformer 1 is the most stable conformational isomer, followed by Conformers 2 and 3 (Fig. 2d and Table 1). It is worth noting that Conformers 1 and 2 possess similar ground-state energies. Their energy differences amount to 0.0079–0.0139 eV, which are much smaller than the thermal energy at room temperature (0.0388 eV). These small energy differences indicate that both conformers are largely present in the solution of **DPTB**. Moreover, although the energy differences between Conformers 1 and 3 increase to 0.0427–0.0492 eV, these discrepancies are still comparable to the thermal energy at room temperature. We thus expect the presence of a small amount of Conformer 3 in the solution of **DPTB** as well.

Interestingly, our theoretical calculations are corroborated by crystallographic experiments. The crystal structure of **DPTB** resembles the molecular structure of Conformer 1 (Fig. 2e, f; Fig. S3 and Table S1, ESI†). This is not surprising, as our theoretical calculations show that Conformer 1 is the most stable conformer.

More importantly, our computational results show that these conformers exhibit distinct electronic structures and optical spectra. Although the difference in their calculated UV-Vis absorption peaks is very small (~5 nm), their theoretical emission peaks vary up to ~40 nm (Table 2). Conformers 2 and 3 exhibit blue-shifted peak emission wavelengths with respect to Conformer 1. Consequently, the thermal equilibrium of these conformers is expected to enable single-fluorophore ratiometric imaging.

Table 1 Relative energy levels (eV) of Conformers 2 and 3 with respect to that of Conformer 1 in the ground state in various environments

Conformers	*In vacuo*	Cyclohexane	EA	Ethanol	DMSO
Conformer 2	0.0079	0.0103	0.0127	0.0137	0.0139
Conformer 3	0.0427	0.0439	0.0480	0.0490	0.0492

Table 2 Calculated peak UV-Vis absorption/emission wavelengths (nm) and oscillator strengths (in round brackets) of Conformers 1–3 *in vacuo*, and in cyclohexane, EA, ethanol, and DMSO

Conformers	*In vacuo*	Cyclohexane	EA	Ethanol	DMSO
Absorption					
Conformer 1	361 (0.4196)	368 (0.5331)	367 (0.5299)	367 (0.5207)	367 (0.5314)
Conformer 2	356 (0.7490)	363 (0.9755)	363 (0.9518)	363 (0.9460)	363 (0.9680)
Conformer 3	355 (1.0456)	363 (1.3721)	362 (1.3400)	362 (1.3327)	363 (1.3646)
Emission					
Conformer 1	438 (0.1524)	439 (0.2471)	447 (0.3866)	447 (0.3638)	445 (0.3182)
Conformer 2	401 (0.8123)	416 (1.0261)	431 (1.2115)	439 (1.2933)	440 (1.3060)
Conformer 3	400 (0.9528)	416 (1.1922)	431 (1.3786)	439 (1.4567)	440 (1.4683)

Moreover, our oscillator strength data show that Conformers 2 and 3 are more emissive than Conformer 1. When higher temperature populates more Conformers 2 and 3, **DPTB** may even exhibit brighter emissions.

Finally, we have also considered solvent effects by performing quantum chemical calculations in four solvents (Table 1). It is worth noting that the energy difference between Conformer 1 and the other conformers increases as solvent polarity increases. Increasing temperature may thus play a more critical role in polar solvents than *in vacuo* and in non-polar solvents, to effectively facilitate conformational conversions.

Experimental validations of ground-state conformers

The presence of multiple conformational isomers is supported by fluorescence lifetime measurements (Table 3). In ethanol, emission data reveal two major lifetime components ($\tau_1 \approx 6.5$ ns and $\tau_2 \approx 10.5$ ns), which are assigned to Conformers 1 and 2. In the blue end of the fluorescence spectrum (430 nm), we also noticed the emergence of the third lifetime component but with a small contribution ($\tau_3 \approx 2.9$ ns), which is likely linked to Conformer 3. Similar lifetime data are also found in other solvents (Table S2, ESI†).

To verify if these conformers appear in the ground state, we collected the fluorescence spectra of **DPTB** in ethanol. By exciting this sample at various wavelengths, we expect to see a gradually shifting emission peak if multiple conformers co-exist and exhibit different UV-Vis absorption/emission spectra in the solution. Indeed, we observed a consistent shift of the emission peak from 476 to 478 nm (Fig. 3a).

Furthermore, we probed the fluorescence excitation spectra of this sample at emission wavelengths of 440 and 540 nm, respectively (Fig. 3b and Fig. S4, S5, ESI†). These two spectra maximize at 417 and 421 nm, respectively. Their distinct profiles demonstrate that the conformers indeed exist in the ground state of **DPTB**, in good agreement with our theoretical predictions (Table 2).

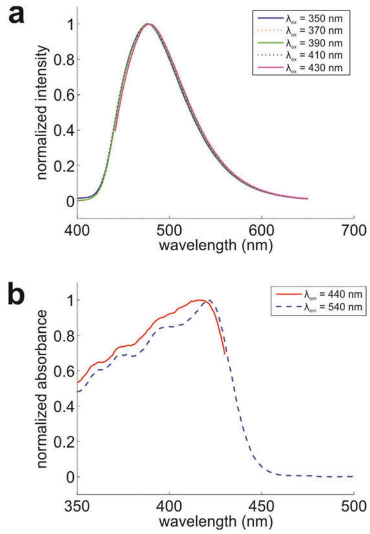

Fig. 3 (a) Normalised fluorescence spectra of **DPTB** in ethanol at room temperature, excited at various wavelengths from 350 to 430 nm. (b) Normalised fluorescence excitation spectra of **DPTB** in ethanol at room temperature, monitored at emission wavelengths of 440 and 540 nm, respectively ([**DPTB**] = 5 μM).

Table 3 Double-exponential fitting to the fluorescence decay dynamics of **DPTB** in ethanol at various emission wavelengths (λ_{em}). **DPTB** was excited at 370 nm; τ: lifetime; RC: relative contribution

λ_{em}	τ_1 (ns)	RC (%)	τ_2 (ns)	RC (%)	χ^2
430	2.86	16.36	9.34	83.64	1.45
480	6.43	28.55	10.34	71.45	1.20
530	6.61	34.84	10.57	65.16	1.17
580	6.48	34.42	10.50	65.58	1.44
650	6.43	35.73	10.58	64.27	1.20

Given the presence of multiple conformers of **DPTB**, we also examined their NMR spectra (see the ESI†). Interestingly, NMR data of **DPTB** do not show a distinct spectrum of each conformer, but only their overall features. These data indicate that **DPTB** conformers can freely convert in the ground state and are all accessible at room temperatures.

Temperature dependence of absorption and emission spectra

Inspired by the co-existence of multiple conformers, we studied the temperature dependence of the UV-Vis and emission spectra of **DPTB** in cyclohexane, EA, ethanol, and DMSO (Fig. 4). The selected solvents have different properties. The results collectively reflect the impact of solvent effects on the equilibrium between conformational isomers.

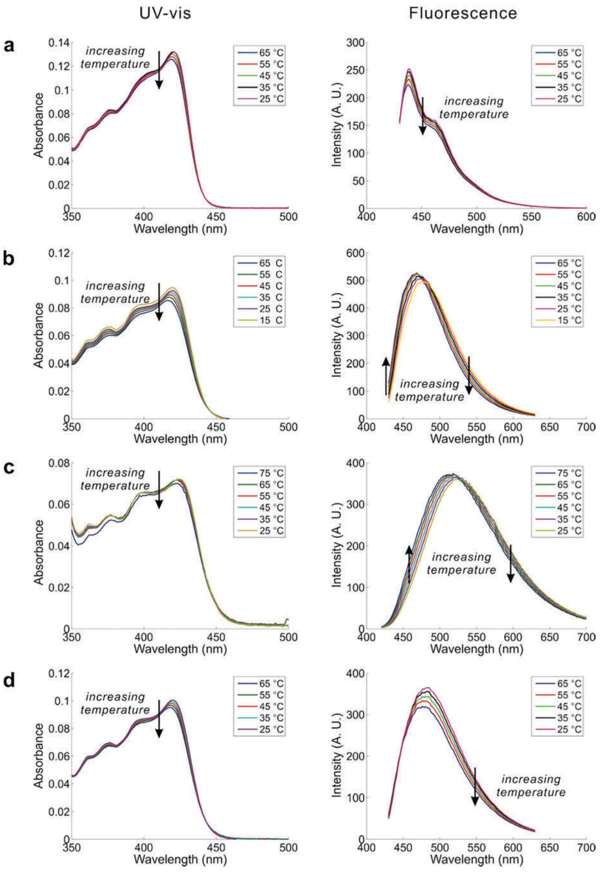

Fig. 4 UV-Vis absorption and fluorescence spectra of **DPTB** in (a) cyclohexane (excited at 415 nm); (b) EA; (c) DMSO and (d) ethanol. ([**DPTB**] = 5 μM; fluorescence spectra were excited at 420 nm, unless stated otherwise).

In all tested solvents, the first absorption band of the UV-Vis absorption spectra extends from 350 to 470 nm, with a peak around 420 nm in **DPTB**. The associated solvatochromism is very weak, as evident from the minimal variation in peak absorption wavelengths of **DPTB** from cyclohexane to DMSO. This observation is in good agreement with the theoretical calculations. However, a close examination shows that there is a subtle blue shift in the UV-Vis absorption peaks. We also noticed that the peak absorbance of **DPTB** in all solvents experiences a slight drop as the temperature increases.

The blue shift with increasing temperature is much obvious in the emission spectra of **DPTB**. In general, long-wavelength emissions of **DPTB** exhibit a decrease in intensity as the temperature increases. In contrast, short-wavelength emissions of **DPTB** remain stable or even become enhanced at high temperatures. Consequently, these changes in the emission profiles of **DPTB** lead to a noticeable blue-shift (*i.e.*, by ~10 nm over a temperature increase of 50 °C in both EA and DMSO).

The blue shifts in fluorescence spectra of **DPTB** are consistent with our theoretical calculations. That is, Conformers 2 and 3, which exhibit a hypsochromic shift with respect to Conformer 1, populate as the temperature increases.

DPTB displays bright fluorescence in all tested solvents, with outstanding quantum yields (>40%, Table S3, ESI†).

Interestingly, the peak emission intensities of **DPTB** demonstrate an atypical positive temperature coefficient in DMSO (0.06% per °C) and EA (0.11% per °C) (Fig. 4b, c and Table S4, ESI†). This unusual feature is not surprising, considering that the quantity of more emissive Conformers 2 and 3 increases, while that of less emissive Conformer 1 drops with increasing temperature.

In contrast, the peak emission intensities of **DPTB** in cyclohexane and ethanol consistently drop with temperature increase (Fig. 4a and d). On one hand, the thermal equilibrium of conformation isomers indeed favours more emissive Conformers 2 and 3 at high temperatures. On the other hand, rising temperature reduces the quantum yields of all conformers, owing to enhanced radiationless de-excitations. Perhaps in cyclohexane and ethanol, the decrease in quantum yield plays a more significant role. Consequently, **DPTB** displays a negative temperature coefficient. These results show that solvent effects have an important impact on the overall temperature-dependence of **DPTB** emissions.

Fluorescent thermometer applications

Thermal equilibrium of conformational isomers and their distinct emission profiles permit the deployment of **DPTB** as a fluorescent thermometer (Fig. 5). **DPTB** allows ratiometric temperature measurements based on a single type of fluorophore. As the thermal equilibrium of these ground-state conformers is governed by the Boltzmann distribution and not affected by the dye concentration, their ratiometric readings are inherently independent of photobleaching. **DPTB** based fluorescent thermometers are thus highly reliable, and particularly suitable for long-lasting applications.

Indeed, our experiments show that the temperature calibration curves of **DPTB** in various solvents exhibit excellent statistical goodness-of-fit (Fig. 5a–c).

To demonstrate the usefulness of **DPTB** in temperature sensing, we have injected its ethanol solution into a small channel embedded in a PDMS chip (Fig. 5d and e). This flexible device is semi-transparent under ambient light, and highly emissive under UV radiation (Table S3, ESI†). This device in combination with a portable spectrometer and the calibration curve (Fig. 5c) allows convenient temperature measurements.

To further demonstrate the simplicity of **DPTB** as a thermometer, we use a standard digital camera to capture raw images of this dye in DMSO under UV excitation at different temperatures (Fig. 5f). While the colour and intensity changes are relatively subtle to the naked eye, the ratio of intensities in the blue and green channels of these raw images affords useful information about the temperatures (Fig. 5g).

This fluorescent system also demonstrates excellent reversibility and reliability. During 10 heating/cooling cycles between 25 °C and 75 °C, the measured fluorescence intensities are extremely consistent (Fig. S6, ESI†). We also placed this system under continuous UV irradiation for 24 hours at 25 °C. The corresponding fluorescence intensities remained the same throughout the course.

It is worth highlighting that not only **DPTB**, but also many other pseudo-rigid fluorophores are expected to possess

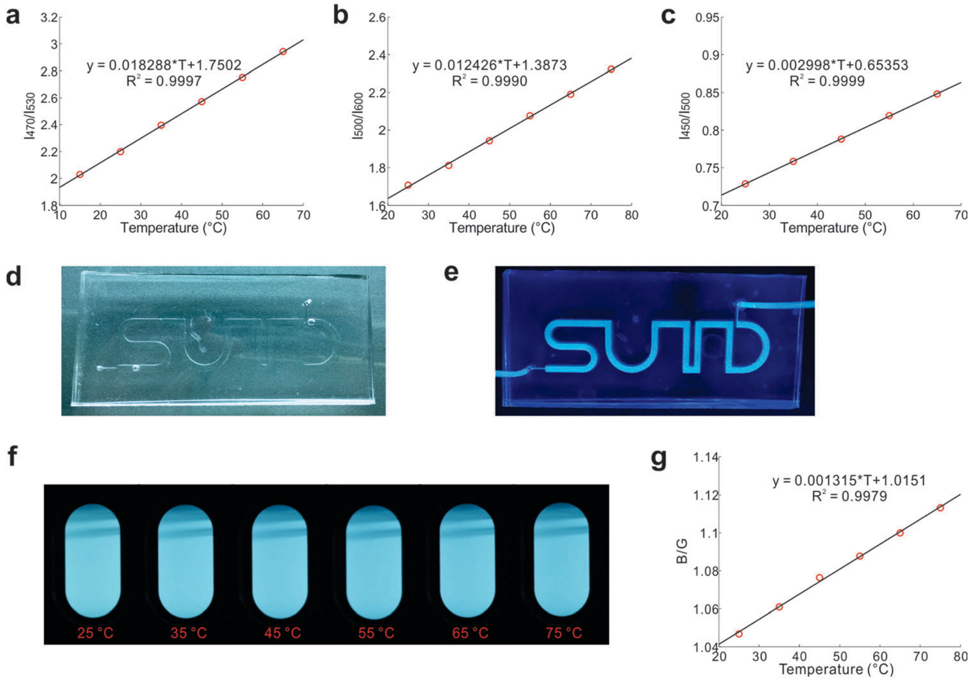

Fig. 5 The temperature-dependence of emission intensity ratios and the associated best-fit equations of **DPTB** in (a) EA (the ratio of intensities at 470 and 530 nm); (b) DMSO (the ratio of intensities at 500 and 600 nm); and (c) ethanol (the ratio of intensities at 450 and 500 nm). Photographs of **DPTB** in ethanol under (d) ambient light and (e) UV radiation in the dark. (f) Photographs of **DPTB** in DMSO at different temperatures. (g) Temperature calibration curve based on the intensity ratios of blue (B) and green (G) channels in the photographs in (f). ([**DPTB**] = 5 μM).

multiple accessible conformers in the ground state.[41–43] These fluorophores could allow photobleaching-independent ratiometric temperature measurements. And their availability demonstrates the generality of our design strategy to realize single-fluorophore ratiometric thermometers.

Finally, thermometry based on these fluorophores is best suited in solvents, when temperature is the only factor affecting fluorophore conformations. In the presence of other interference factors (such as biomolecules), these fluorophores can be capped inside polymer nanoparticles to serve as dedicated temperature sensors.[8,41] Note that conformational changes of fluorophores are still feasible in polymers with large free volume.

Conclusion

We have demonstrated a strategy to achieve a single-fluorophore ratiometric thermometer, based on ground-state conformers of **DPTB**. These conformers are present at room temperature and exhibit different emission spectra. Consequently, thermal equilibrium of these conformers enables ratiometric temperature sensing with simple design and high reliability. Such a single-fluorophore ratiometric thermometer overcomes the reliability issue related to varied photobleaching rates in dual-fluorophore ratiometric thermometers. Moreover, unlike conformational changes in the excited state (that generally quench fluorescence and afford weak fluorescence), these ground state conformational isomers emit bright signals. Finally, as more emissive conformers become populous at high temperatures, **DPTB** even exhibits an unusual positive temperature coefficient in ethyl acetate and DMSO. We expect that employing ground state conformational isomers will open a new door for developing highly reliable ratiometric imaging systems.

Computational and experimental details

DFT calculations were performed using Gaussian 09.[44] Hybrid functional wB97XD and the 6-31G(d,p) basis set were used for all calculations. The geometry optimizations of various conformational isomers of **DPTB** in both their ground and the first excited singlet states (S_0 and S_1) were performed *in vacuo*, and in cyclohexane, EA, ethanol, and DMSO. Frequency checks in the ground state were conducted after each geometry optimization to ensure that minima on the potential energy surfaces (PES) were found. Following this, TD-DFT calculations were carried out on the optimized molecular structures to determine their peak absorption/emission wavelengths and oscillator strength (using linear response solvation). Solvent effects, when applicable, were treated using the C-PCM model.

DPTB was a gift from Yang Laboratory, and its synthesis procedures were reported previously (Fig. S7 and S8, ESI†).[40]

A single crystal of **DPTB** suitable for X-ray structural analysis was obtained by slow evaporation from a chloroform/*n*-hexane solution at room temperature. Single crystal X-ray diffraction intensity data were collected on a Xcalibur Gemini ultra-diffractometer using the ω-scan mode with graphite-monochromator Mo Kα radiation (0.71073 Å). The crystal was kept at 293(2) K during data collection. Using Olex2,[45] the structure was solved with the Superflip program[46] and refined with the SHELXL package.[47]

^{1}H-NMR and ^{13}C-NMR spectra were recorded on a Bruker 400 spectrometer, using TMS as an internal standard. Chemical shifts were given in ppm and coupling constants (J) in Hz.

The fluorescence lifetime of **DPTB** in various solvents was measured using a Fluoromax-4 spectro-fluorometer equipped with a NanoLED-370 pulsed diode (excitation wavelength, 368 nm) and a DeltaHub TCSPC controller.

Fluorescence spectra were collected using a Cary Eclipse spectrometer equipped with a Peltier temperature controller. Emission spectra of **DPTB** in cyclohexane, EA, ethanol, and DMSO were measured at different temperatures ranging from 15 °C to 75 °C. Readings were taken at a 30 min interval to ensure that samples had reached the desired temperatures before each measurement. A Cary 60 spectroscope was used to collect the UV-Vis absorption spectra of all samples in the same temperature range as that of fluorescence spectra.

The quantum yields of **DPTB** in cyclohexane, EA, ethanol, and DMSO were determined *via* the relative determination method, with Coumarin 153 as a reference compound.[48]

A minichannel with alphabets "SUTD" was designed using AutoCAD® 2016. The width and height of the channel were 1.7 mm x 1.7 mm. The CAD designed geometry was then printed using the Stereolithography (SLA) based Form 2™ (Formlabs, USA) 3D printer using Clear™ resin with a layer thickness of 0.025 mm. The 3D printed mold was post-processed by isopropanol wash for 10 min followed by UV curing for 1 h. For replica molding of the post processed mold, a mixture of poly(dimethylsiloxane) (PDMS) prepolymer (Sylgard 184 Silicone Elastomer kit, Dow Corning, USA) and its curing agent in the ratio of 10 : 1 was prepared. The PDMS mixture was then degassed under vacuum in a desiccator for removal of entrapped bubbles. The degassed PDMS was then cast over the mold and oven baked at 60 °C for 24 h. The heat cured PDMS was then removed from the mold with the channels being replicated, and provisions for flow inlet and outlet were made using a 1 mm hole puncher. The fabricated PDMS replica mold was then bonded to thin slabs of PDMS to form sealed channels *via* plasma bonding.

Conflicts of interest

There are no conflicts of interest to declare.

Acknowledgements

The authors thank Professor Guoqiang Yang from the Institute of Chemistry, Chinese Academy of Sciences, for helpful discussions. This work is supported by Singapore University of Technology and Design (T1SRCI17126), Singapore-MIT Alliance for Research and Technology, the National Natural Science Foundation of China (21422606 and 21402191) and Dalian Cultivation Fund for Distinguished Young Scholars (2014J11JH130 and 2015J12JH205).

References

1 X.-D. Wang, O. S. Wolfbeis and R. J. Meier, *Chem. Soc. Rev.*, 2013, **42**, 7834–7869.
2 Z. Yang, J. Cao, Y. He, J. H. Yang, T. Kim, X. Peng and J. S. Kim, *Chem. Soc. Rev.*, 2014, **43**, 4563–4601.
3 J. Sakakibara and R. J. Adrian, *Exp. Fluids*, 1999, **26**, 7–15.
4 D. Ross, M. Gaitan and L. E. Locascio, *Anal. Chem.*, 2001, **73**, 4117–4123.
5 R. Fu, B. Xu and D. Li, *Int. J. Therm. Sci.*, 2006, **45**, 841–847.
6 A. J. Bur, M. G. Vangel and S. Roth, *Appl. Spectrosc.*, 2002, **56**, 174–181.
7 A. Nakano, J. Luo and A. Ros, *Anal. Chem.*, 2014, **86**, 6516–6524.
8 K. Okabe, N. Inada, C. Gota, Y. Harada, T. Funatsu and S. Uchiyama, *Nat. Commun.*, 2012, **3**, 705.
9 S. Arai, S.-C. Lee, D. Zhai, M. Suzuki and Y. T. Chang, *Sci. Rep.*, 2014, **4**, 6701.
10 S. Arai, M. Suzuki, S.-J. Park, J. S. Yoo, L. Wang, N.-Y. Kang, H.-H. Ha and Y.-T. Chang, *Chem. Commun.*, 2015, **51**, 8044–8047.
11 J. Jenkins, S. M. Borisov, D. B. Papkovsky and R. I. Dmitriev, *Anal. Chem.*, 2016, **88**, 10566–10572.
12 S. Collins, G. Baxter, S. Wade, T. Sun, K. Grattan, Z. Zhang and A. Palmer, *J. Appl. Phys.*, 1998, **84**, 4649–4654.
13 S. Ebert, K. Travis, B. Lincoln and J. Guck, *Opt. Express*, 2007, **15**, 15493–15499.
14 V. Natrajan and K. Christensen, *Meas. Sci. Technol.*, 2008, **20**, 015401.
15 P. Löw, B. Kim, N. Takama and C. Bergaud, *Small*, 2008, **4**, 908–914.
16 X. Liu, D. Mao, J. M. Cole and Z. Xu, *Chem. Commun.*, 2014, **50**, 9329–9332.
17 Z. R. Grabowski, K. Rotkiewicz and W. Rettig, *Chem. Rev.*, 2003, **103**, 3899–4032.
18 Y. Hong, J. W. Y. Lam and B. Z. Tang, *Chem. Soc. Rev.*, 2011, **40**, 5361–5388.
19 J. Mei, N. L. Leung, R. T. Kwok, J. W. Lam and B. Z. Tang, *Chem. Rev.*, 2015, **115**, 11718–11940.
20 X. Liu, Z. Xu and J. M. Cole, *J. Phys. Chem. C*, 2013, **117**, 16584–16595.
21 C. Yuan, S. Saito, C. Camacho, S. Irle, I. Hisaki and S. Yamaguchi, *J. Am. Chem. Soc.*, 2013, **135**, 8842–8845.
22 D. Su, C. L. Teoh, L. Wang, X. Liu and Y.-T. Chang, *Chem. Soc. Rev.*, 2017, **46**, 4833–4844.
23 X. Liu, Q. Qiao, W. Tian, W. Liu, J. Chen, M. J. Lang and Z. Xu, *J. Am. Chem. Soc.*, 2016, **138**, 6960–6963.
24 J. B. Grimm, B. P. English, J. Chen, J. P. Slaughter, Z. Zhang, A. Revyakin, R. Patel, J. J. Macklin, D. Normanno, R. H. Singer, T. Lionnet and L. D. Lavis, *Nat. Methods*, 2015, **12**, 244–250.
25 C.-J. Ou, X.-H. Ding, Y.-X. Li, C. Zhu, M.-N. Yu, L.-H. Xie, J.-Y. Lin, C.-X. Xu and W. Huang, *J. Phys. Chem. C*, 2017, **121**, 14803–14810.
26 J. Kim and T. M. Swager, *Nature*, 2001, **411**, 1030–1034.
27 H. Zhang, Z. Zhang, J. Zhang, K. Ye, H. Gao and Y. Wang, *CrystEngComm*, 2007, **9**, 951–958.

28 Z. Chi, X. Zhang, B. Xu, X. Zhou, C. Ma, Y. Zhang, S. Liu and J. Xu, *Chem. Soc. Rev.*, 2012, **41**, 3878–3896.

29 Q. Qi, J. Zhang, B. Xu, B. Li, S. X.-A. Zhang and W. Tian, *J. Phys. Chem. C*, 2013, **117**, 24997–25003.

30 W. Z. Yuan, Y. Tan, Y. Gong, P. Lu, J. W. Y. Lam, X. Y. Shen, C. Feng, H. H. Y. Sung, Y. Lu, I. D. Williams, J. Z. Sun, Y. Zhang and B. Z. Tang, *Adv. Mater.*, 2013, **25**, 2837–2843.

31 K. Wang, H. Zhang, S. Chen, G. Yang, J. Zhang, W. Tian, Z. Su and Y. Wang, *Adv. Mater.*, 2014, **26**, 6168–6173.

32 Y. Zhang, Q. Song, K. Wang, W. Mao, F. Cao, J. Sun, L. Zhan, Y. Lv, Y. Ma, B. Zou and C. Zhang, *J. Mater. Chem. C*, 2015, **3**, 3049–3054.

33 Y. Xu, K. Wang, Y. Zhang, Z. Xie, B. Zou and Y. Ma, *J. Mater. Chem. C*, 2016, **4**, 1257–1262.

34 Y. Xu, Z. Xie, H. Zhang, F. Shen and Y. Ma, *CrystEngComm*, 2016, **18**, 6824–6829.

35 A. G. Szabo and D. M. Rayner, *J. Am. Chem. Soc.*, 1980, **102**, 554–563.

36 J. Saltiel, D. Sears Jr, J. Choi, Y. Sun and D. Eaker, *J. Phys. Chem.*, 1994, **98**, 35–46.

37 A. Szemik-Hojniak, J. M. Zwier, W. J. Buma, R. Bursi and J. H. van der Waals, *J. Am. Chem. Soc.*, 1998, **120**, 4840–4844.

38 J. Saltiel, D. F. Sears, Y. P. Sun and J. O. Choi, *J. Am. Chem. Soc.*, 1992, **114**, 3607–3612.

39 L. D. Lavis and R. T. Raines, *ACS Chem. Biol.*, 2008, **3**, 142–155.

40 J. Feng, K. Tian, D. Hu, S. Wang, S. Li, Y. Zeng, Y. Li and G. Yang, *Angew. Chem., Int. Ed.*, 2011, **50**, 8072–8076.

41 J. Feng, L. Xiong, S. Wang, S. Li, Y. Li and G. Yang, *Adv. Funct. Mater.*, 2013, **23**, 340–345.

42 X. Liu, S. Li, J. Feng, Y. Li and G. Yang, *Chem. Commun.*, 2014, **50**, 2778–2780.

43 Q. Fang, J. Li, S. Li, R. Duan, S. Wang, Y. Yi, X. Guo, Y. Qian, W. Huang and G. Yang, *Chem. Commun.*, 2017, **53**, 5702–5705.

44 M. Frisch, G. Trucks, H. B. Schlegel, G. Scuseria, M. Robb, J. Cheeseman, G. Scalmani, V. Barone, B. Mennucci and G. Petersson, *et al.*, *Gaussian 09*, Gaussian Inc., Wallingford, CT, 2009.

45 O. V. Dolomanov, L. J. Bourhis, R. J. Gildea, J. A. Howard and H. Puschmann, *J. Appl. Crystallogr.*, 2009, **42**, 339–341.

46 L. Palatinus and G. Chapuis, *J. Appl. Crystallogr.*, 2007, **40**, 786–790.

47 G. M. Sheldrick, *Acta Crystallogr., Sect. C: Struct. Chem.*, 2015, **71**, 3–8.

48 C. Würth, M. Grabolle, J. Pauli, M. Spieles and U. Resch-Genger, *Nat. Protoc.*, 2013, **8**, 1535–1550.